



This is a repository copy of *Mechanism of Hydrogen-Bonded Complex Formation between Ibuprofen and Nanocrystalline Hydroxyapatite.*

White Rose Research Online URL for this paper:

<https://eprints.whiterose.ac.uk/113895/>

Version: Published Version

Article:

Ryabenkova, Y, Jadav, N, Conte, M. et al. (5 more authors) (2017) Mechanism of Hydrogen-Bonded Complex Formation between Ibuprofen and Nanocrystalline Hydroxyapatite. *Langmuir*, 33 (12). pp. 2965-2976. ISSN 0743-7463

<https://doi.org/10.1021/acs.langmuir.6b04510>

This document is the Accepted Manuscript version of a Published Work that appeared in final form in *Langmuir*, copyright © American Chemical Society after peer review and technical editing by the publisher. To access the final edited and published work see: <https://doi.org/10.1021/acs.langmuir.6b04510>.

Reuse

This article is distributed under the terms of the Creative Commons Attribution (CC BY) licence. This licence allows you to distribute, remix, tweak, and build upon the work, even commercially, as long as you credit the authors for the original work. More information and the full terms of the licence here: <https://creativecommons.org/licenses/>

Takedown

If you consider content in White Rose Research Online to be in breach of UK law, please notify us by emailing eprints@whiterose.ac.uk including the URL of the record and the reason for the withdrawal request.



eprints@whiterose.ac.uk
<https://eprints.whiterose.ac.uk/>

Mechanism of Hydrogen-Bonded Complex Formation between Ibuprofen and Nanocrystalline Hydroxyapatite

Yulia Ryabenkova,[†] Niten Jadav,[‡] Marco Conte,[§] Michael F. A. Hippler,[§] Nik Reeves-McLaren,^{||} Phil D. Coates,[†] Peter Twigg,[†] and Anant Paradkar^{*,‡,§}

[†]School of Engineering, University of Bradford, Bradford, BD7 1DP, United Kingdom

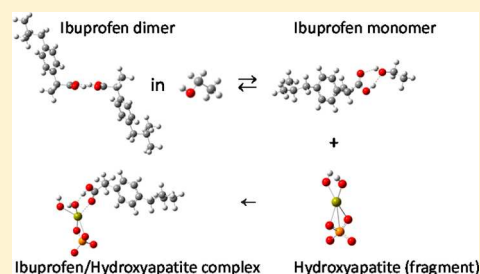
[‡]Centre for Pharmaceutical Engineering Science, School of Pharmacy, University of Bradford, Bradford, BD7 1DP, United Kingdom

[§]Department of Chemistry, University of Sheffield, Sheffield, S3 7HF, United Kingdom

^{||}Department of Materials Science and Engineering, University of Sheffield, Sheffield, S1 3JD, United Kingdom

S Supporting Information

ABSTRACT: Nanocrystalline hydroxyapatite (nanoHA) is the main hard component of bone and has the potential to be used to promote osseointegration of bone implants and to treat bone defects. Here, using active pharmaceutical ingredients (APIs) such as ibuprofen, we report on the prospects of combining nanoHA with biologically active compounds to improve the clinical performance of these treatments. In this study, we designed and investigated the possibility of API attachment to the surface of nanoHA crystals via the formation of a hydrogen-bonded complex. The mechanistic studies of an ibuprofen/nanoHA complex formation have been performed using a holistic approach encompassing spectroscopic (Fourier transform infrared (FTIR) and Raman) and X-ray diffraction techniques, as well as quantum chemistry calculations, while comparing the behavior of the ibuprofen/nanoHA complex with that of a physical mixture of the two components. Whereas ibuprofen exists in dimeric form both in solid and liquid state, our study showed that the formation of the ibuprofen/nanoHA complex most likely occurs via the dissociation of the ibuprofen dimer into monomeric species promoted by ethanol, with subsequent attachment of a monomer to the HA surface. An adsorption mode for this process is proposed; this includes hydrogen bonding of the hydroxyl group of ibuprofen to the hydroxyl group of the apatite, together with the interaction of the ibuprofen carbonyl group to an HA Ca center. Overall, this mechanistic study provides new insights into the molecular interactions between APIs and the surfaces of bioactive inorganic solids and sheds light on the relationship between the noncovalent bonding and drug release properties.



1. INTRODUCTION

Hydroxyapatite (abbreviated as HA), with its chemical formula $\text{Ca}_{10}(\text{PO}_4)_6(\text{OH})_2$, is a major inorganic component of bone and, along with collagen fibrils, it accounts for up to 65% of the hard tissue of vertebrates. Bone-derived hydroxyapatite is nanosized, nonstoichiometric, calcium-deficient carbonated ceramic material with low crystallinity.¹ Synthetic poorly crystalline nanoscale HA that mimics the composition of natural bone has long been employed in orthopedics for the treatment of bone defects resulting from trauma or surgery, because it possesses excellent biocompatibility and osteoconductivity properties,² thus showing a great potential for use in bone tissue engineering³ and implant osseointegration,⁴ as well as being a potential gene⁵ or drug carrier.^{6,7}

Drug delivery systems based on ceramics,^{8,9} polymers,¹⁰ or hydrogels¹¹ have received an enhanced interest in the last decades. HA-based ceramic drug carriers, in turn, have been particularly studied as prospective drug delivery systems for the treatment of bone infection,^{12,13} as well as arthritis.¹⁴ Osteoarthritis and rheumatoid arthritis, despite having different causes behind the diseases, share similar symptoms of chronic pain due to associated peripheral inflammation. Both are

considered to be important public health concerns,¹⁵ with osteoarthritis being the most common cause for total hip or knee replacement. The results of total arthroplasty in arthritic patients shows that HA-coated prostheses have excellent medium-term efficacy,¹⁶ promoting osseointegration and, in turn, opening up the prospects of using bioactive ceramics as drug carriers for the treatment of bone diseases.

One of the most common analgesic anti-inflammatory nonsteroidal drugs used for the relief of pain symptoms in arthritic patients is ibuprofen.¹⁷ Ibuprofen, or 2-(4-isobutylphenyl) propanoic acid (Figure 1a), exists as a cyclic hydrogen-bonded dimer in a solid state (Figure 1b),¹⁸ and its anti-inflammatory and analgesic activity is assigned to the monocarboxyl groups of an ibuprofen monomer.¹⁹ Based on this, it is beneficial to introduce ibuprofen into the body as a monomer, for instance as a sodium salt,²⁰ for an improved performance due to a higher drug solubility.

Received: December 21, 2016

Revised: February 15, 2017

Published: March 7, 2017

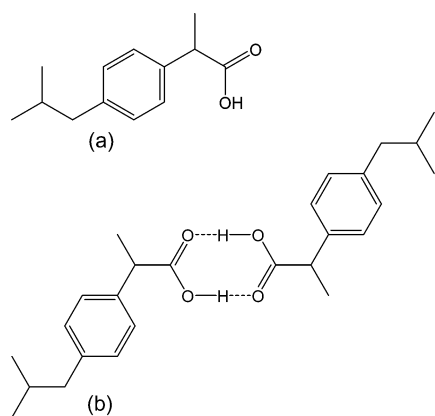


Figure 1. Structures of (a) ibuprofen monomer, 2-(4-isobutylphenyl) propanoic acid, and (b) dimer of ibuprofen highlighting the hydrogen bond between carboxyl groups.

Several attempts have been made to combine HA and ibuprofen for treating bone-associated diseases, possibly in a monomeric state to achieve the desired drug dissolution rates.^{21,22} These studies attempt to relate the prolonged retention times and drug release either with the geometry of the materials²³ or with the porosity of ceramics,²⁴ in combination with hydrogen bonding effects between HA and ibuprofen monomer. While the majority of studies produced materials using a trial-and-error approach to determine the best possible combination of an API and an excipient, they did not focus on the mechanism of the API adsorption and release, but rather on the final formulation with certain characteristics. However, to the best of our knowledge, there are currently no insights into the physical chemistry behind the ibuprofen loading onto the surface of hydroxyapatite and its release. In this paper, we report, for the first time, on mechanistic studies that describe the adsorption of ibuprofen on the surface of HA and propose a possible mechanism for the interaction of ibuprofen and hydroxyapatite at the molecular level. The understanding of the surface properties of ceramics and its influence on the API dissolution rates may provide a useful conceptual platform for the rational development and design of formulations with the desired controlled and sustained drug release.

2. MATERIALS AND METHODS

2.1. Nanohydroxyapatite Preparation. Nanohydroxyapatite was prepared as reported in ref 25 and references therein. In brief, calcium hydroxide ($\text{Ca}(\text{OH})_2$) (3.704 g, assay $\geq 96\%$, Sigma–Aldrich) and phosphoric acid (H_3PO_4) (3.459 g, 85 wt % in water, Sigma–Aldrich) were dissolved in 100 mL of deionized water each. The solution of phosphoric acid was fed into the solution of calcium hydroxide at room temperature using a peristaltic pump at a rate of 3 mL min^{-1} . The resulting slurry was left under constant stirring for 2 h for aging and left overnight for settling. The top aqueous layer was then removed and the suspension was dried at 60°C and subsequently ground using an agate mortar and pestle to form a powder. A portion of the powder was calcined for 2 h in a furnace at 1000°C (with a heating rate of $10^\circ\text{C min}^{-1}$) in order to evaluate its thermal stability.

2.2. Ibuprofen/Nanohydroxyapatite Complex Synthesis. To prepare an ibuprofen/HA complex, the following procedure was employed. Ibuprofen (200 mg, grade 70 UPS/EP, Albemarle) was dissolved in anhydrous ethanol (5 mL, absolute 99%+, Fisher) in a 19/26 joint 100 mL round-bottom flask. A sample of dried as-prepared nanoHA (800 mg) was added to the solution and stirred in a Buchi Rotavapor at 30°C and 350 mbar for 1 h at a speed of 60 rpm. The

temperature then was increased to 45°C and the pressure was reduced to 175 mbar to reach the condition of a very viscous paste (to avoid complete evaporation of ethanol). The reproducibility of the method was evaluated using ATR-FTIR experiments for each sample to confirm the presence of monomeric, dimeric, and attached species (where applicable). The reason behind opting for the 20 wt % loading is explained in the Supporting Information (Figure S1). An aliquot of the paste was used for *in situ* and *ex situ* spectroscopic studies, whereas the remaining part was dried at room temperature for 24 h and used for morphological examination.

2.3. Materials Characterization. Fourier transform infrared (FTIR) spectra were acquired using a ThermoFisher Nicolet iS50 FTIR spectrophotometer that was equipped with a single reflection diamond attenuated total reflection (ATR) module. Spectra were recorded in the absorbance mode from 4000 cm^{-1} to 375 cm^{-1} at 1 cm^{-1} resolution, averaging 64 scans.

Powder X-ray diffraction (PXRD) patterns were acquired using a Bruker D8 Avance diffractometer operating at 40 kV and 40 mA with $\text{Cu K}\alpha$ radiation. In order to minimize preferred orientation of crystallites within specimens, PXRD data were collected in Debye–Scherrer mode for ibuprofen-containing samples mounted in silica glass capillaries using a PANalytical X’Pert³ powder diffractometer with $\text{Cu K}\alpha$ radiation, operating at 45 kV, 40 mA, and a Medipix³ Pixel1D detector. The samples were analyzed in the range of either 20° – $60^\circ 2\theta$ for nanoHA characterization or from 0° – $80^\circ 2\theta$ for ibuprofen and ibuprofen/HA complexes. Analysis of the obtained patterns was carried out using X’Pert HighScore Plus software, and stripping of the $\text{K}\alpha_2$ component was carried out when appropriate. Crystallite sizes for the HA were determined using the Scherrer equation,²⁶ and XRPD patterns were compared with entries of the International Centre for Diffraction Data (ICDD) Powder Diffraction File (PDF).

Raman spectra were obtained using a home-built Raman spectrometer, as described in ref 27, but with the following modifications: using a frequency doubled Nd:YAG laser, 532.2 nm, 20 mW (Lasos, GL3dT) and a monochromator (Andor SR-163) equipped with 1200 l/mm grating, 500 nm blaze, and cooled CCD camera (Andor i-Dus, -60°C). Effective slit width is given by a $100 \mu\text{m}$ core diameter fiber. Wavenumber calibration was performed using Ne emission lines and known benzene Raman transitions (NIST database²⁸). Experimental resolution was $\sim 8 \text{ cm}^{-1}$, and the full width at half-maximum (fwhm) was $\sim 1700 \text{ cm}^{-1}$. With regard to Raman shifts, the Raman peak position accuracy was estimated to be $\pm 3 \text{ cm}^{-1}$.

Scanning electron microscopy (SEM) images were recorded using a Hitachi Model TM3000 electron microscope operating at 15 kV. All samples were sputtered with gold prior to analysis.

Dissolution experiments were performed using a UPS II type Labindia dissolution tester (Model Labin-09, India). Ibuprofen/HA complex, physical mixture of ibuprofen and HA or raw ibuprofen powders were placed at the bottom of the dissolution vessel (at least four repeats) containing 900 mL phosphate buffer (pH 7.2) maintained at $37 \pm 0.5^\circ\text{C}$ and stirred with a paddle at 50 rpm. Samples were collected periodically and further filtered. Quantification of ibuprofen was performed spectrophotometrically at a fixed wavelength of 221 nm, using a Jasco Model V630 spectrophotometer.

^1H NMR experiments were recorded at 400 MHz using a Bruker Avance III 400 spectrometer. Measurements were collected at room temperature for solutions of ibuprofen in CDCl_3 or $\text{CD}_3\text{CD}_2\text{OD}$ (Sigma–Aldrich). Fitting of the NMR peaks was carried out using Bruker TopSpin 3.2 software, and data analysis was carried out by using a successive approximation method based on a fixed-point iteration algorithm.

2.4. Computational Studies. Quantum chemical calculations were performed using Gaussian 09, version D.01.²⁹ A density functional theory (DFT)³⁰ method using the B3LYP functional and a 6-311G(d,p) basis set (Pople triple split valence Gaussian basis functions with added polarization functions) for all atoms have been employed.³¹ The nature of stationary states (minimum structures) was confirmed by frequency calculations. Stabilization energies of the complexes were obtained by subtraction from energetic values of isolated species and considering zero-point-energy (ZPE) correc-

Table 1. Unit-Cell Parameters from Rietveld Refinement and Crystallinity Evaluations of NanoHA As-Synthesized and Calcined at 1000 °C^a

material	Unit-Cell Parameters (Å)			unit-cell volume, V (Å ³)	crystallite size (nm)	crystallinity (%)	HA phase purity (wt %)
	a	b	c				
HA raw	9.439	9.439	6.887	531.4 ± 1.1	13	35	100
HA calcined	9.403	9.403	6.876	526.5 ± 1.1	79	96	77 ^b

^aContraction of the unit cell upon calcination is observed as well as increase in crystallinity. A second phase, namely tri-calcium phosphate or TCP, has also been detected after thermal treatment, showing non-stoichiometry of the as-prepared HA. ^b23 wt % attributed to the tricalcium phosphate (JCPDS File No. 9-169).

tions³² for all of the molecular structures. Calculated wavenumbers to compare with experimental infrared spectra were obtained from harmonic vibrational frequencies using the B3LYP density functional method with the 6-311G(d,p) basis set by introducing a scaling factor of 0.9616.³³

3. RESULTS AND DISCUSSION

3.1. NanoHA Characterization. The inorganic part of bone is mainly made of a nanodimensional nonstoichiometric poorly crystalline HA phase with small inclusions of carbonate.¹ Several characterization techniques were employed to verify whether the synthesized ceramics mimic the bone composition. Figure S2 in the Supporting Information shows the XRD pattern of both as-prepared and calcined HA. It can be seen that the raw material (Figure S2a) is made solely of HA phase that fully matches JCPDS File No. 9-432 (for a visualization of its unit cell, see Figure S3 in the Supporting Information). The broad reflection peaks on the XRD patterns in the region between 20° and 50° 2θ are usually characteristic of either partially amorphous or nanoparticulate material. Interestingly, Figure S2b reveals that the composition of the materials has changed after calcination. Besides the main phase of HA, another phase of tricalcium phosphate, or TCP (JCPDS File No. 9-169), appeared. This is caused by the decomposition of the nonstoichiometric HA into β-calcium phosphate.³⁴ Crystallinity calculations, in turn, showed that the raw, or as-prepared HA, is composed of ca. 35% crystalline component, whereas the crystallinity of the calcined HA expectedly reached ca. 96% after a prolonged heat treatment (Table 1).

According to the Rietveld refinement results for the lattice parameters, the calculated unit cell of the raw HA was 531.4 ± 1.1 Å³, whereas for the calcined material, it was 526.5 ± 1.1 Å³, while the proportion of the second phase of tricalcium phosphate (TCP) was 23 wt %. The Scherrer equation²⁶ allowed us to evaluate the crystallite size, which appeared to be 13 nm for raw HA and 79 nm for calcined HA. Decomposition of HA into TCP after thermal treatment and reduction of the unit cell volume is indirect evidence of its nonstoichiometry, whereas its particle (crystallite) size lies within a nanometer range, thus proving that the HA used for this study is indeed a nonstoichiometric nanosized material with poor crystallinity.

To further prove its similarity to the HA in the bone, we used an attenuated total reflectance (ATR) FTIR technique, since XRD alone, being a bulk method, cannot reveal all of the details of the HA composition, especially for the layers of solid close to its surface. ATR-FTIR is a spectroscopic technique where an IR beam is directed at a solid sample and is further reflected to a detector.³⁵ An important aspect of this method is that this technique is often regarded as a “surface” method with a penetration depth in the range of 0.5–3 μm.³⁶ That is, the method is a surface technique when compared to XRD, but not a pure surface analysis method like X-ray photoelectron

spectroscopy, which probes 0.5–10 nm instead. However, considering that (i) our HA is present in the form of agglomerates ranging from 20 μm to 200 μm and (ii) ibuprofen is also in a similar range (*vide infra*; see Figure 3), we can ascribe the use of ATR-FTIR as a surface method, but with a large penetration depth. This particular aspect of the technique will be important also for the investigation of the mechanism of adsorption of ibuprofen to the HA surface (see section 3.4.4).

An ATR-FTIR spectrum of raw hydroxyapatite is reported in Figure S4 in the Supporting Information. The main active bands lie in the region of 1100–400 cm⁻¹, with the typical phosphate stretching bands lying in the range of 1200–900 cm⁻¹, as well as at ~600 cm⁻¹, being in agreement with previously published data, hydroxyl group vibrations are located at 3571 and 632 cm⁻¹.^{37–39} Minor carbonate substitution of B-type (CO₃²⁻ for PO₄³⁻) was also detected with the corresponding peaks for bending and stretching modes at 870 cm⁻¹ and 1600–1300 cm⁻¹, respectively, thus suggesting that the surface carbonate formation occurred during the preparation, despite the fact that carbonate anions were not deliberately introduced into the system. This is a known phenomenon where CO₂ capture from the atmosphere may occur when one of the solutions has high pH values⁴⁰ or a strongly basic surface in the presence of moisture. Overall, the presence of small amounts of carbonate groups on the surface of HA is characteristic for the wet precipitation preparation method. However, our results are slightly different from previously reported studies where it has been suggested that A-type carbonate substitution (CO₃²⁻ for OH⁻) occurs at lower temperatures, whereas B-type substitution is a feature of the materials prepared at elevated temperature ranges.²⁵ We observed only a slightly detectable A-type substitution with the B-type dominating, thus suggesting that the material mostly mimics the young bone tissue,⁴¹ as the ratio of A/B types is age-dependent and also influences the HA crystallinity and solubility.⁴²

3.2. Ibuprofen/HA Complex Formation. In order to prepare an ibuprofen–HA complex, we opted for dissolution of the API in ethanol with subsequent solvent evaporation under vacuum and deposition of ibuprofen onto the ceramic’s surface while drying in a Rotavapor.⁴³ The reason behind such a choice is 2-fold. First, ethanol is a much more “green” solvent, with minimal environmental impact in chemical production, compared to the widely used hexane, yet it still allows successful solubilization of ibuprofen. Second, the solvent evaporation process allows us to control the API loading and eliminates the need of postprocessing the API content measurement (as in the case of immersion of HA into hexane with dissolved ibuprofen²¹), since there is no API loss during the preparation and the ibuprofen uptake is independent of the porosity properties of the ceramic.

With the objective of evaluating the possibility of API attachment to the surface of HA, we employed a wide variety of methods. First, we wanted to assess the homogeneity of the ibuprofen distribution on the surface of ceramics. [Figure 2](#)

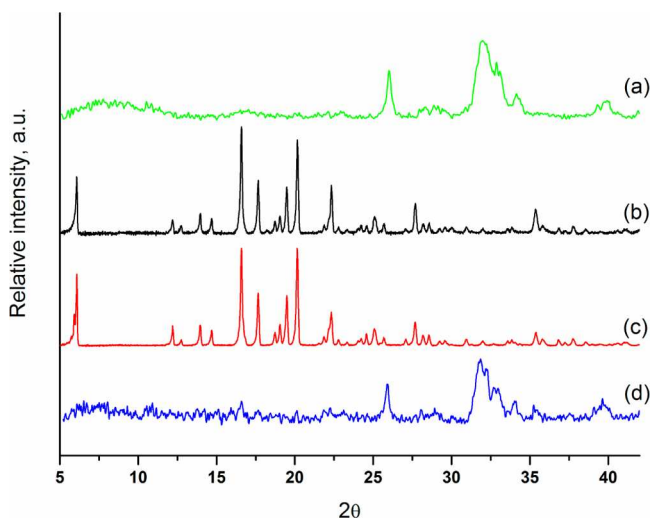


Figure 2. PXRD patterns of (a) raw HA, (b) commercial, or as received, ibuprofen from the supplier, (c) commercial ibuprofen recrystallized in ethanol, (d) ibuprofen/hydroxyapatite (ibuprofen/HA) complex. The pattern of ibuprofen/HA complex is similar to that of pure HA, no peaks of ibuprofen detected, suggesting a thin layered structure. Patterns (b) and (c) for crystalline ibuprofen have been scaled down for better visualization purposes.

shows the comparison of XRD patterns between as-prepared HA ([Figure 2a](#)), pure ibuprofen from the supplier ([Figure 2b](#)), ibuprofen recrystallized from ethanol using the method of ibuprofen/HA complex preparation with the ceramic addition

step being omitted ([Figure 2c](#)), and the ibuprofen–hydroxyapatite complex itself ([Figure 2d](#)).

As can be seen from the patterns, while both commercial and ethanol recrystallized ibuprofen specimens are highly crystalline (full match with the JCPDS database entry 32-1723), the ibuprofen/HA complex does not exhibit any reflections characteristic of ibuprofen but shows only broad reflections of a poorly crystalline HA phase. The absence of ibuprofen reflections on the XRD patterns in general can be explained by any of the following reasons: (i) amorphous or low crystalline component, (ii) particle size below 4–5 nm, and (iii) highly dispersed thin layered structure. In our case, we can eliminate the amorphous phase formation because, in the case of ethanol-recrystallized ibuprofen, a highly crystalline material was observed ([Figure 2c](#)); therefore, the most probable explanation of the absence of the ibuprofen reflections in the ibuprofen/HA complex pattern is the presence of a well dispersed thin layer of ibuprofen or small particles.

SEM also revealed some interesting findings. [Figure 3](#) shows the micrographs of raw HA ([Figure 3A](#)), commercial ibuprofen ([Figure 3B](#)), ibuprofen after ethanol recrystallization ([Figure 3c](#)), and ibuprofen/HA complex ([Figure 3D](#)).

It can be seen that raw HA consists of reasonably large agglomerates of ca. 200 μm and some smaller clusters of 10–20 μm . Commercial ibuprofen showed rod-shaped particles of ca. 50–200 μm , whereas ethanol-recrystallized ibuprofen particles are randomly shaped with the average size ranging from 10 μm to 250 μm . We do not exclude the possibility of the formation of rod-shaped particles with larger dimensions during the recrystallization of ibuprofen, as the recrystallized sample is crushed in a mortar and pestle prior to analysis, and this may not be a complete representation of the particle shape and size. However, we need to compare the ethanol treated ibuprofen specimen with the ibuprofen/HA complex that has also been ground to reach a powder form, and we believe the comparison

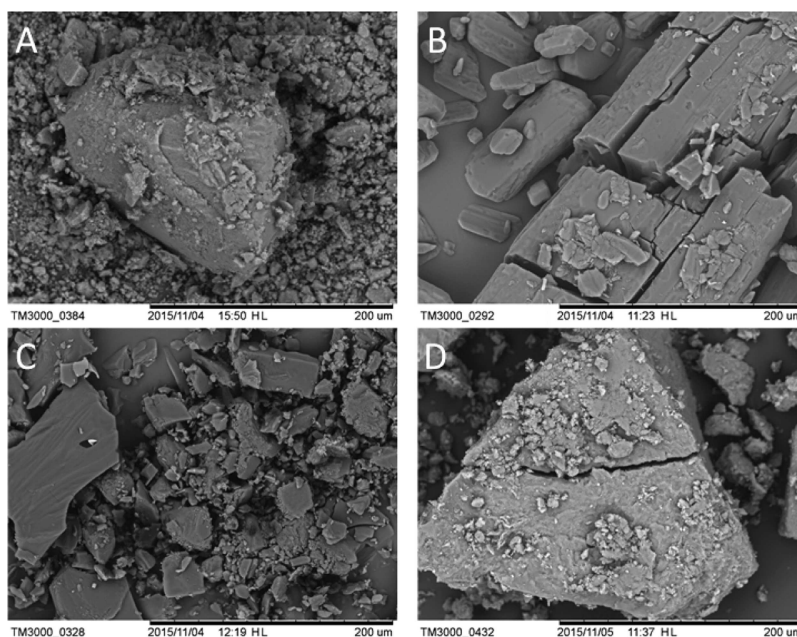


Figure 3. SEM micrographs of (A) raw HA, (B) commercial, or as-received, ibuprofen from the supplier, (C) commercial ibuprofen recrystallized in ethanol, and (D) ibuprofen/hydroxyapatite (ibuprofen/HA) complex. Similar particle shapes and sizes were observed for as-prepared HA (panel (a)) and ibuprofen/HA complex (d).

between two SEM micrographs for these materials is valid in this case.

Another interesting feature observed during the SEM analysis was specimen destruction under the electron beam (Figure S5 in the Supporting Information). Structural damage upon irradiating the sample with the beam of electrons is a well-known phenomenon and may happen not just with organic samples⁴⁴ but also with ceramics, although at much higher accelerated voltages and current densities.⁴⁵ We decided to exploit this feature to try to visualize the presence of ibuprofen in our ibuprofen/HA complex. In other words, if the ibuprofen recrystallized in the presence of HA to form large clusters like it does in the absence of ceramics (Figure 3C), ibuprofen particles would be damaged upon prolonged (30 s or more) exposure to the 15 kV electron beam. However, if the ibuprofen forms a thin layer on the entire surface of the HA, it would be much harder to detect electron beam damage upon exposure. After careful inspection of the specimen of ibuprofen/HA complex under SEM at different magnifications and various irradiation times (Figure S5) we were not able to detect any structural deformation. Thus, by using a “negative proof” approach of deliberate prolonged irradiation of the specimen with an electron beam and comparing it with bulk ibuprofen behavior in SEM under the same conditions, we demonstrated that our material is indeed a thin layered structure. While bulk ibuprofen was easily damaged by the beam, we did not find any areas of beam damage for the Ibu/HA samples, thus suggesting that no large areas of ibuprofen clusters were formed during the synthesis, and our material is most likely a homogeneous mixture of ibuprofen and HA, with the former creating a thin layer on the surface of HA. This observation is more indirect evidence of a highly dispersed thin layer of API on the surface of HA, rather than a biphasic space separated API–ceramic system, thus complementing our earlier XRD findings.

Further insights into the complex formation can be obtained using ATR-FTIR spectroscopy. Figure 4 shows the spectra of ibuprofen/HA complex (spectrum in Figure 4a) and ethanol-treated ibuprofen (spectrum in Figure 4b).

The majority of active bands are in the ranges of 1800–500 cm^{-1} and 3200–2400 cm^{-1} , with the former assigned to carbonyl group, tertiary and quaternary carbon atoms, and OH bending vibrations, and latter to the C–H and C–C bond stretching.⁴⁶ Interestingly, overlapping of the two spectra (see inset on Figure 4) clearly shows the shift of the ibuprofen C=O group stretching to the higher wavenumbers from 1707 cm^{-1} to 1717 cm^{-1} . Similar shifts have been reported in the literature, and they are usually explained, yet not proved, by the hydrogen bonding between the hydroxyl group of HA and the carbonyl group of ibuprofen. However, the degree of this deviation was variable from study to study, ranging from 1720 cm^{-1} ¹²⁴ to 1547 cm^{-1} .²³ This large variability in literature data, as well as the lack of direct evidence on the actual nature of molecular bond interactions between ibuprofen and HA, prompted us to investigate this issue in more detail.

3.3. Fourier Transform Infrared (FTIR) Studies of Ibuprofen Monomer, Dimer, and Attached/Chemisorbed Species. First, we decided to evaluate the behavior of ibuprofen in ethanol solution. It is known that ibuprofen exists in a hydrogen-bonded cyclic dimeric form that is stable in both solid and liquid phases.¹⁸ We aimed to verify the possibility of the existence of the ibuprofen monomer in the ethanol solution as we employed this solvent for our studies. To do so, we dissolved ibuprofen crystals in absolute ethanol

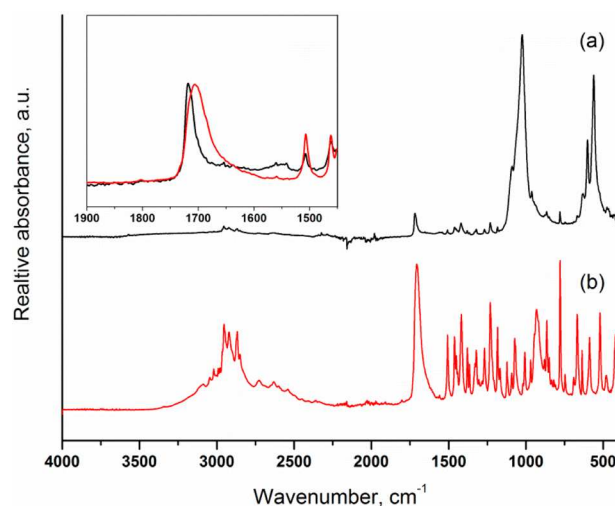


Figure 4. ATR-FTIR spectra of ibuprofen/HA complex (spectrum in Figure 4a) and ibuprofen recrystallized in ethanol (spectrum in Figure 4b). Inset shows carbonyl region of ibuprofen spectra (normalized) clearly indicating the shift in frequency of ibuprofen/HA complex to higher wavenumbers (1717 cm^{-1}), compared to pure ibuprofen (1707 cm^{-1}).

and deposited the resulting solution dropwise onto the ATR crystal of the ATR–FTIR spectrometer and allowed it to dry naturally, taking measurements at the beginning and end of the experiment. Figure S6a in the Supporting Information shows the IR spectrum at the zero time point measurement in the presence of ethanol, whereas Figure S6b in the Supporting Information shows the spectrum of ibuprofen after 4 h when the ethanol had completely evaporated (as indicated by the absence of ethanol’s most active bands at 880, 1046, and 1087 cm^{-1} and a broad band between 3600 and 3000 cm^{-1}). What is immediately apparent is the presence of a broad shoulder in the region between 1760 and 1720 cm^{-1} in the spectrum corresponding to the ibuprofen dissolved in ethanol (Figure S6a). Deconvolution of this part of the spectrum (see inset in Figure S6) allowed us to determine the peak position of a second species, which appeared to be at ca. 1735 cm^{-1} and has been assigned as the C=O stretching vibration of monomer ibuprofen affected by hydrogen bonding with ethanol (further confirmed by the computational studies). Thus, we have proven that ibuprofen may exist in both dimeric and monomeric forms when ethanol is present in the system.

In order to provide semiquantitative information for the amounts of monomer and dimer in solution that will be useful for our data treatment for adsorbed species, the equilibrium constant ($K_{\text{eq,D}}$) for the process $2 \times \text{M} \rightarrow \text{D}$ was determined by NMR, where M represents the monomer and D the dimer. This determination was carried out in chloroform to minimize the proton exchange and, in turn, line broadening, and, therefore, the visibility of the proton of the COOH group of ibuprofen involved in the dimer formation. As monomer and dimer are in fast exchange regime, the signal of the proton for the COOH group will appear as a single broad peak. Its position is dependent on the amount of monomer and dimer by the correlation: $\delta_{\text{m}} = \delta_{\text{M}}P_{\text{M}} + \delta_{\text{D}}P_{\text{D}}$,⁴⁷ where δ_{m} represents the measured average position of the proton involved in the monomer/dimer equilibrium, δ_{M} is an extrapolated position for the sole monomer, δ_{D} an extrapolate peak position for the dimer, and P_{M} and P_{D} the populations of monomer and dimer

expressed in molar fraction, with the condition $P_M + P_D = 1$. Initial estimates for δ_M and δ_D were used to evaluate P_D iteratively (full details are given in the Supporting Information (Figures S7–S13)).

By using this approach, a $K_{\text{eq,D,CDCl}_3}$ value of $[D]/[M]^2 = 116$ was determined, thus showing the existence of large amounts of a dimer in solution. We consider this value to be an upper limit, with respect to the same equilibrium in ethanol. In fact, because of competing line broadening for the proton on COOH with the OH group of ethanol, it is not possible to extract this information directly in ethanol solutions. On the other hand, by using this same approach, it is possible to provide a crude estimate for the value of equilibrium constant for the process $M + \text{EtOH} \rightarrow M/\text{EtOH}$ via analysis of the shift of ethanol signal in ibuprofen-containing solutions. By using the same approach on peak position analysis, with $\delta_m = \delta_{\text{EtOH}}P_{\text{EtOH}} + \delta_{M/\text{EtOH}}P_{M/\text{EtOH}}$ a rough estimate of $K_{\text{eq,EtOH}} = [M/\text{EtOH}]/([M] \cdot [\text{EtOH}]) = 0.8$ was obtained, thus showing the existence of both monomer and dimer in solution.

Therefore, having assessed the presence of ibuprofen monomer in the ethanol solution, the next step was to evaluate the presence of dimer, monomer, and possible adsorbed species, in the ibuprofen/HA complex that we synthesized, using time-online IR spectroscopic measurements. An *in situ* experiment was carried out, using an as-prepared ibuprofen/HA complex specimen that was transferred directly from the preparation flask onto the ATR crystal of the spectrometer. Measurements were taken at various time points (from 6 min to 180 min) and we did not observe any peak at 1717 cm^{-1} (as in Figure 4 above), a band that we believe corresponds to the adsorbed monomeric ibuprofen species.

To investigate this phenomenon, we performed *ex situ* measurements where the specimens were taken from the preparation flask at given time points and transferred onto the ATR crystal instead (Figure 5).

This is different from the previous, *in situ*, IR experiment, because, in the first case, the specimen is always the same across the experiment, whereas, in this second case, the specimens are different at every measurement time point, although still originating from the same ibuprofen/HA sample (flask).

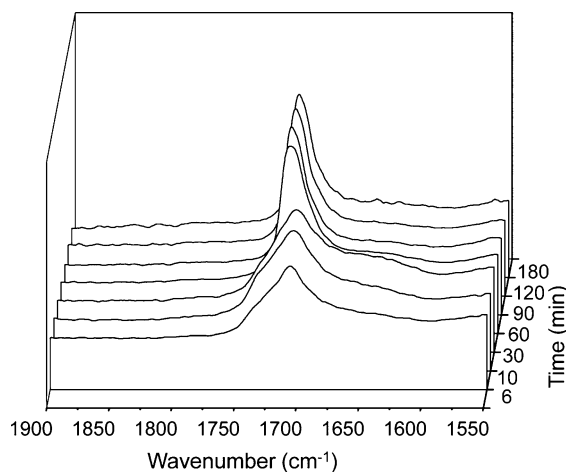


Figure 5. Kinetics of the ibuprofen/HA complex formation, *ex situ* ATR-FTIR measurements of the carbonyl region of ibuprofen between 6 and 180 min, showing the evolution of the peak assigned as attached species, and the signal decay of the dimer and monomer peaks.

Interestingly, in the case of *ex situ* kinetic studies, we were able to observe a peak at 1717 cm^{-1} instead. This suggests that keeping a specimen between the force applicator and the ATR crystal for the entire duration of the *in situ* experiment (180 min) prevents the formation of the adsorbed species, leading only to the recrystallization of the ibuprofen dimer.

3.4. Mechanistic Studies and Molecular Modeling. The data gathered using *ex situ* time-online infrared studies for the ibuprofen/HA complex prompted us to investigate and describe a possible mechanism for the intermolecular complex formation by using a combination of computational studies, as well as FTIR and Raman spectroscopies.

Computational studies were carried out using density functional theory and a B3LYP functional, using 6-311G(d,p) basis set for all other atoms. Our model considers the energetics of an ibuprofen monomer versus a more stable dimeric species and the interaction that this monomer can have with an HA adsorption site.

3.4.1. Energetics and Structures of Ibuprofen Monomer and Dimer. Ibuprofen is a molecule that can exist in several conformers. By using a B3LYP/6-31G(d) level of theory, De Carvalho and co-workers identified eight stable minima.⁴⁶ Of these conformers, the most stable and the one best matching IR data was a structure presenting the carboxyl and isobutyl groups of the ibuprofen molecule on opposite sides, with respect to the plane of the benzene ring. Employing this structural element as a starting point, we optimized this structure using a higher level of theory for structure optimization (B3LYP/6-311G(d,p)), and obtained the structure reported in Figures 6a and 6b. This has been used as a model for the formation of an ibuprofen dimer, as well as ibuprofen/HA interactions in our study.

For completeness, we should mention that we identified a further minimum (Figures 6c and 6d) close in energy to the previous one, with an energy gap of $+15 \text{ kJ mol}^{-1}$. This energy gap is reasonably small and the two species might both exist in

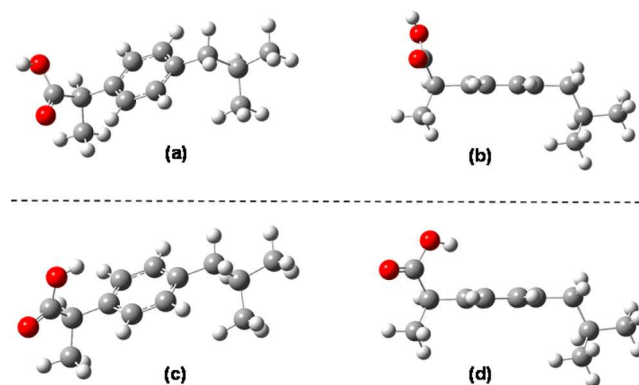


Figure 6. Ibuprofen structure optimized using a DFT/B3LYP/6-311G(d,p) level of theory: (a and b) absolute minimum with (a) ibuprofen view from top highlighting the carboxyl group, and (b) ibuprofen view from side to highlight the relative position of carbonyl and isopropyl groups with respect to the benzene ring. (c and d) relative minimum for a conformer obtained by rotation of the carbonyl group along a C–C axis from structure (a). For this second structure: (c) view from top highlighting the rotation of the carbonyl group, and (d) view from a side with respect to the benzene ring plane. Note the orientation of the hydroxyl group with the H atom pointing to the benzene ring, underlying an intramolecular hydrogen bond. Color code: (red atoms) oxygen, (gray atoms) carbon, (white atoms) hydrogen.

solution. We think this second minimum exists by virtue of an intramolecular hydrogen bond between the H atom of the hydroxyl group and the benzene ring⁴⁸ (Figure 6d). However, since this conformer is less stable, and it would not be able to form a dimer, because of the orientation of the hydroxyl group pointing to the benzene ring, it will not be considered further in our discussion.

Using the conformer in Figures 6a and 6b, we first determined the structure of an ibuprofen dimer. In principle, two dimeric forms can be postulated: a *cis* form, with the carbon skeletons of the two ibuprofen molecules facing each other, or a *trans* form, where the carbon skeletons of the two molecules are in the opposite direction, with respect to the plane identified by the carboxylic groups of ibuprofen. In this study, only the *trans* dimer has been considered as it is the most stable and its existence has been proved in the solid state.¹⁸ Using our model, the *trans* dimer (Figure S14 in the Supporting Information) has a stabilization energy, with respect to two isolated molecules of ibuprofen, of -69 kJ mol^{-1} . This indicates a strong hydrogen-bond interaction between the OH and CO groups of the carboxyl unit of a molecule of ibuprofen with the CO and OH groups, respectively, of another molecule of ibuprofen (see Figure S14).

Conversely, it also shows that the process of dissociation of a dimer to two units of monomer is not spontaneous. However, as in our experiments, ibuprofen is dissolved in ethanol, and we detected the existence of an IR band at 1735 cm^{-1} (see section 3.3) when both ibuprofen and ethanol are present, we can assume that this solvent promotes the dimer dissociation into two monomer units. That is the formation of an ibuprofen/ethanol complex in solution via the reaction: $D + 2\text{EtOH} \rightarrow 2M/\text{EtOH}$ (where D and M stand for dimer and monomer, respectively). A stable hydrogen-bonded M/EtOH complex was identified (Figure S15 in the Supporting Information) and the energetics of this dissociation reaction assisted by ethanol was calculated to be -29 kJ mol^{-1} and thus favored.

Note that our IR data identify a peak at 1735 cm^{-1} that is observed in the presence of ethanol only. With our data, we think that we can assign this peak to an ibuprofen/ethanol complex, as expected in the dissolution process.

3.4.2. Hydroxyapatite (HA) Adsorption Site. In order to mimic hydroxyapatite and ibuprofen interaction, an adsorption site was built. This site was constructed by using a simplified, yet useful, model comprising the most distinct features of HA in place of an entire hydroxyapatite crystal. These features are the presence of a phosphate group bound to a calcium atom presenting two hydroxyl groups (Figure S16 in the Supporting Information).

In order to validate whether this neutral HA fragment is representative for our studies, we calculated the position of IR bands for stretching and bending motions of the phosphate group, and for the libration motion of the OH groups (which are also bound to a single Ca center in a HA crystal). Our model calculates these vibrations at 1036, 411, and 608 cm^{-1} , respectively. Experimental values for these same vibrations are 1020, 443, and 632 cm^{-1} .⁴⁹ Taking into account that our simplified model does not include lattice parameters, the calculated wavenumber values are in good agreement with experimental data, and, as such, we consider it to be a good platform for the investigation of ibuprofen and HA interactions.

3.4.3. Ibuprofen and Hydroxyapatite (HA) Interactions. From the ibuprofen and HA structures described in sections 3.4.1 and 3.4.2 (and Figures 6 and Figure S16), an adsorption

complex between ibuprofen and HA was built. A stable minimum with a large stabilization energy of -133 kJ mol^{-1} was found (see Figure S17 in the Supporting Information).

This minimum presents a hydrogen bond interaction between ibuprofen and HA. However, and quite interestingly, this hydrogen-bond interaction occurs between the OH group of the carboxyl function of ibuprofen ($\text{HO}_{\text{ibuprofen}}$) and the hydroxyl groups of the HA bound to Ca ($\text{HO}_{\text{apatite}}$) in a $\text{HO}_{\text{apatite}} \cdots \text{HO}_{\text{ibuprofen}}$ interaction. That is, this bond does not involve a hydrogen bond between the CO group of ibuprofen ($\text{CO}_{\text{ibuprofen}}$) and the OH group of the hydroxyapatite ($\text{HO}_{\text{apatite}}$) in a $\text{CO}_{\text{ibuprofen}} \cdots \text{HO}_{\text{apatite}}$ interaction, but the carbonyl group appears to interact with the apatite via a Ca center, as a $\text{CO}_{\text{ibuprofen}} \cdots \text{Ca}_{\text{apatite}}$ instead. As such, two anchoring points for ibuprofen are present via $\text{HO}_{\text{apatite}}$ and $\text{Ca}_{\text{apatite}}$ centers.

In the other words, a hydrogen bond is present and, as such, fits current tentative explanations of ibuprofen and HA interactions;²³ however, in our case, this is an $\text{HO}_{\text{apatite}} \cdots \text{HO}_{\text{ibuprofen}}$ hydrogen-bond interaction, and not a $\text{CO}_{\text{ibuprofen}} \cdots \text{HO}_{\text{apatite}}$ hydrogen-bond interaction.²³ Furthermore, our model also suggests that changes in vibrational frequencies of the C=O group of ibuprofen are also due to the existence of a non-hydrogen-bond, $\text{CO}_{\text{ibuprofen}} \cdots \text{Ca}_{\text{apatite}}$ interaction.

For this complex, we calculated a C=O vibrational frequency of 1694 cm^{-1} . This correctly predicts a red shift of $\sim 50 \text{ cm}^{-1}$, with respect to an isolated monomeric species (expected at 1746 cm^{-1}). However, our level of theory does not allow an unambiguous assignment of IR bands from the spectra as the dimer is also calculated in the 1694 cm^{-1} region. However, in this context, it is worth noting that such an interaction is not unusual between a carboxyl group and a metal center and it has been observed in the case of species containing Zn,⁵⁰ where the carboxyl group binds via the carbonyl unit in a monodentate manner, and it also might be operating in our case.

Raman scattering is sensitive to changes in polarizability⁵¹ and, therefore, has different selection rules, compared to IR absorption, and the two techniques can complement each other. For this specific case, we applied Raman spectroscopy to have a wide splitting between the Raman active symmetric C=O stretching frequency of the dimer, and the C=O stretching vibration of the adsorbed species. The C=O stretching vibrations of the dimer split into the symmetric, Raman-active vibration at lower wavenumber, and the antisymmetric, IR active vibration at higher wavenumber. Whereas in the IR spectrum, the antisymmetric C=O stretching of the dimer partially overlaps with the C=O stretching vibration of the adsorbed monomer, in the Raman spectrum, the vibrations are much more separated, making an assignment and interpretation less ambiguous. Raman spectra for pure ibuprofen, ibuprofen in the presence of ethanol, and a sample from an ibuprofen, ethanol, and HA mixture after drying, are reported in Figure 7.

The most intense peak of this set of spectra is centered at ca. 1610 cm^{-1} and corresponds to the vibration of the C–C bond of the benzyl ring. The weaker peak at 1652 cm^{-1} in the spectrum in Figure 7a corresponds to the symmetric C=O stretching vibration of an ibuprofen dimer.⁵² The presence of this peak must be expected in a sample of pure ibuprofen (Figure 7a), because the dimer is the most stable species in solid form (*vide supra*).

When some ethanol is added to the sample (Figure 7b), the 1652 cm^{-1} dimer band disappears and a new and broad peak in

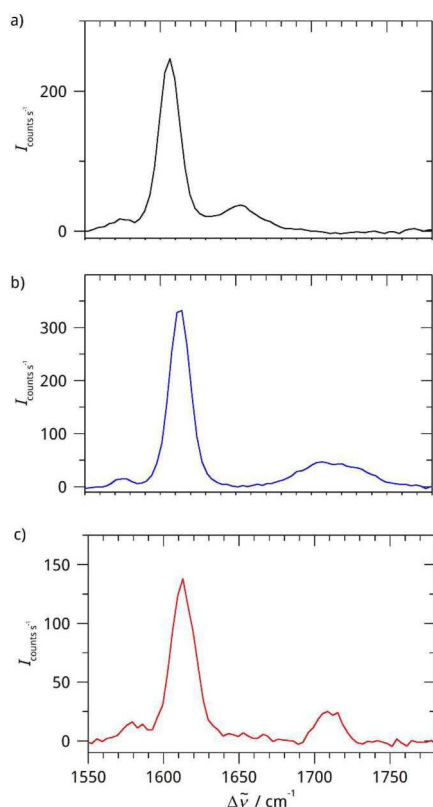


Figure 7. Raman spectra of (a) pure ibuprofen powder, (b) ibuprofen–ethanol solution, and (c) ibuprofen-loaded H-apatite (dry). The most intense band at ca. 1610 cm^{-1} , observed in all spectra, is a C–C stretching vibration of the aryl ring. The band at 1652 cm^{-1} observed in spectrum (a) is the symmetric stretching of the C=O bond in the dimer. The broad band in the region 1700–1730 cm^{-1} in spectrum (b) is for a C=O stretching of ibuprofen in an ibuprofen/ethanol complex. The band at 1710 cm^{-1} for spectrum (c) arises from the C=O stretching of ibuprofen in an ibuprofen/HA complex.

the region 1700–1730 cm^{-1} appears. We ascribe this signal to a C=O stretching vibration of monomer ibuprofen affected by hydrogen bonding with ethanol. In the case of the ibuprofen/HA complex sample (Figure 7c), we can note the presence of a sharper peak at ca. 1710 cm^{-1} that we assign to C=O stretching of an ibuprofen monomer adsorbed to HA, possibly via a C=O \cdots Ca interaction, as described above. In this spectrum, the dimer peak at 1652 cm^{-1} has disappeared, showing that, in this sample, ibuprofen is likely not in the dimer configuration anymore, but mainly bonded to HA. The small but significant shift of the C–C stretching at 1610 cm^{-1} moving from the spectrum in Figure 7a to the spectra in Figures 7b and 7c, reflects a change from a dimer to a monomer.

Considering these assignments, a summary of the stabilization energies of ibuprofen, with respect to dimer, monomer/EtOH, and monomer/HA, which will be useful for our reasoning for the next sections, is reported below (see Figure 8, as well as Table S1 in the Supporting Information).

From the energy diagram, it is possible to observe that any interaction of the monomer with another monomer, ethanol, or HA is always a favorable process. However, the most energetically stable interaction is the one between a monomer of ibuprofen and hydroxyapatite, thus suggesting the formation of an adsorbed species. In addition, the formation of an ibuprofen/ethanol complex is also favored, with respect to the

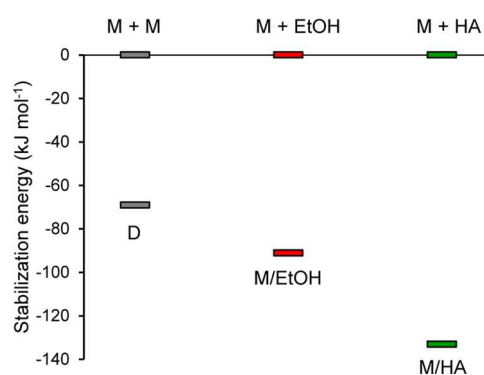


Figure 8. Energy diagram summarizing the stabilization energies for dimer or complexes formation from a monomer of ibuprofen. The symbol “+” stands for two isolated molecules or fragments, the symbol “/” stands for a complex formation. M = ibuprofen monomer, D = dimer, EtOH = ethanol, and HA = hydroxyapatite.

formation of an ibuprofen dimer from two independent monomeric units, and thus supporting a dissolution process and the formation of a monomer under our conditions, as detected in IR (Figure S5 and at 1735 cm^{-1}), and, importantly, the disappearance at 1652 cm^{-1} from Raman spectra (from a dimer) when ethanol is added (Figure 7b) and the formation of a new band in the region of 1700–1730 cm^{-1} .

3.4.4. Kinetics of the Adsorption of Ibuprofen to the Surface of Hydroxyapatite. Having ascertained the presence of an adsorbed ibuprofen species to HA, and with this species possibly presenting a hydrogen bond $\text{HO}_{\text{apatite}}\text{CHO}_{\text{ibuprofen}}$ and a $\text{CO}_{\text{ibuprofen}}\cdots\text{Ca}_{\text{apatite}}$ interaction, we carried out a kinetic study in order to gain an in-depth knowledge of the adsorption process.

From the spectra reported in section 3.3, it is possible to observe a decay of the signal for a M/EtOH species, an increase of an adsorbed ibuprofen species on the HA surface, here denoted M/HA, and an almost-constant signal for the ibuprofen in dimeric form, denoted here as D. The signal intensities are reported in Figure 9.

The almost-constant signal for the bulk ibuprofen dimer D can be easily explained with the working principle of the ATR-FTIR method (see section 3.1).³⁶ This technique is often referred as a surface method, but with a penetration depth of a few micrometers. Therefore, with respect to ibuprofen present

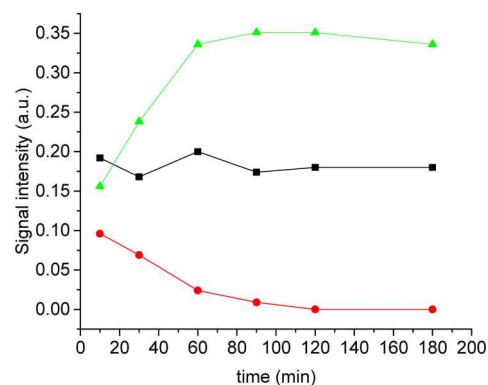
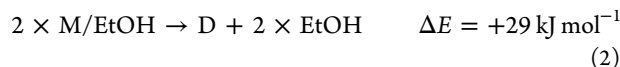
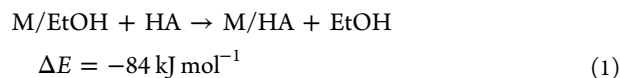


Figure 9. Signal intensity evolution (from ATR-FTIR) against time for (red circles, —●—) ibuprofen monomer (*vide infra*), (black squares, —■—) ibuprofen dimer, and (green triangles, —▲—) monomer adsorbed over HA surface.

in layers such as M/EtOH or M/HA, the ibuprofen presenting a dimer D appears in large excess, and therefore no change in its intensity occurs.

A M/EtOH complex can form an adsorbed species or evolve to a dimer. The energetics for these processes are reported here (per molecule of ibuprofen), in eqs 1 and 2.



Note that if ethanol is taken into account in the process, whereas the adsorption of an ibuprofen molecule is a favorable process (eqs 1 and 2), the formation of a dimer in the presence of ethanol (eq 2) is now an unfavorable process, presenting a small, yet positive, ΔE value (+29 kJ mol⁻¹). This was not the case if the dimer formation was considered without the presence of ethanol (see section 3.4.1), where a stabilization energy of -69 kJ mol⁻¹ was calculated instead.

As a consequence, these data would suggest that the increase in signal that we observe in the spectra in Figure 5 is due to a process involving the evolution of a M/EtOH species to an adsorbed one, M/HA, which is a process now favored, with respect to the formation of a dimer.

In order to experimentally discriminate between the evolution of a monomer M or M/EtOH species to an adsorbed M_{ads} or M/HA against a dimeric species D, we applied a kinetic analysis to the signal decay. In fact, for a monomer that evolves to an adsorbed species, either $\text{M} \rightarrow \text{M}_{\text{ads}}$ or $\text{M/EtOH} + \text{HA} \rightarrow \text{M/HA} + \text{EtOH}$, this would imply a first-order decay of signal I of M/EtOH and a kinetics equal to

$$I_t = I_0 e^{-kt} \quad (3)$$

where I_t is the intensity of the IR signal (absorbance) at time t , k the kinetic constant of the decay process, and I_0 the intensity of the signal at the start of the measurement.

If the monomer M or M/EtOH evolves to a dimer ($\text{D} = 2\text{M}$) instead (or $2 \times \text{M/EtOH} \rightarrow \text{D} + 2\text{EtOH}$), this implies the consumption of two molecules of monomer ($2\text{M} \rightarrow \text{D}$) and, in turn, a second-order kinetics instead. In this case, the process is described by the equation:

$$I_t = \frac{I_0}{1 + ktI_0} \quad (4)$$

Both these models were used to fit the signal decay of the monomeric species (Figure S18 in the Supporting Information). It is possible to observe that a first-order kinetics (Figure S18a) fits the data well for the decay of the monomeric species, unlike a second-order model (Figure S18b), with values of $R^2 = 0.985$ and 0.894 , respectively. We can then conclude that, based on both calculated stability and fitted kinetics, the decay of signal from the monomeric species M/EtOH is consistent with its evolution to an adsorbed species over the HA surface: $\text{M} \rightarrow \text{M}_{\text{ads}}$, for a process: $\text{M/EtOH} + \text{HA} \rightarrow \text{M/HA} + \text{EtOH}$.

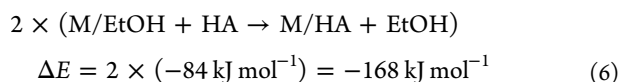
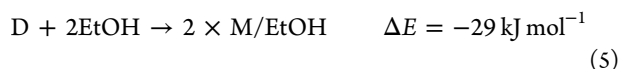
The same principle has been applied for the growth of the signal of the adsorbed species. From the raw data (Figure 9), it also appears that the bare growth of the adsorbed species is 2–3 times greater than the decay of the monomeric species. However, since the signal is related to the absorbance A by the Beer–Lambert law,

$$A = \epsilon bc$$

the signal is also a function of the intrinsic extinction coefficient (ϵ). By using our level of theory, the stretching of the carbonyl group for an adsorbed species is ~ 2 times more intense than the intensity of the signal for an isolated monomer. If we apply this as a correction factor to the growth of the adsorbed species, the kinetics of the growth for the adsorbed species is almost identical to the kinetics of decay of the monomer (see Figure S18).

In order to further corroborate these data, we estimated the equilibrium constant $K_{\text{eq,Ads}}$ for the process $\text{M}_{\text{ads}} \rightarrow \text{M}_{\text{ads}}$ by analyzing the decay of the free monomer and the growth of the adsorbed species. We estimated a value of $K_{\text{eq,Ads}} = [\text{M}_{\text{ads}}]/[\text{M}_{\text{ads}}] = 39$. Note that this value is in the same order of magnitude as the estimated equilibrium constant for the dimer formation in ethanol. We think this is another factor that contributes to our capability to detect and monitor the evolution of a free ibuprofen species to an attached species over the HA surface.

In summary, the adsorption process of an ibuprofen molecule to a site on HA can be schematized as follows:



Net equation:



That is, the adsorption of a monomeric ibuprofen species to an adsorption site of HA is a largely energetically favorable process that occurs in two steps: the dissociation of the ibuprofen dimer to a monomer mediated by ethanol, and the adsorption process to the HA surface via first-order kinetics.

3.5. Dissolution Studies. Finally, we decided to verify how the adsorption of ibuprofen on the surface of hydroxyapatite will influence the drug release properties. Figure 10 shows the drug release profiles of pure ibuprofen (as a control), a physical mixture of ibuprofen and HA, and ibuprofen/HA complex that we proved to be made of a hydrogen bonded API monomer weakly attached to the surface of HA. Figure 10 demonstrates that the drug release of physical mixture is similar to that of a pure ibuprofen, whereas the drug release rate for the ibuprofen/HA complex is statistically slower at the initial time points (between 5 and 180 min) but then equalizes by the 4 h measurement. There have been some reports studying the correlation between the structure and/or porosity of HA versus ibuprofen release.^{23,24} In these studies, the porosity of the system significantly increases the drug retention time, whereas, in our case, we observe only a slight delay in the drug release during the first hour. This could possibly be explained by the fact that the main cause of the retardation of ibuprofen release is due to weak intermolecular bonding between the API and the carrier, and not the geometry of the HA. The intense drug release at the early time points of the dissolution is normally associated with the concentration gradients on the surface, where diffusion pathways are short, followed by the decrease of the drug release rate due to the increase in the diffusion pathways from the bulk. Such formulations are referred to as diffusion-controlled drug delivery system, and the kinetics is based on the known cylindrical geometry of the tablets and

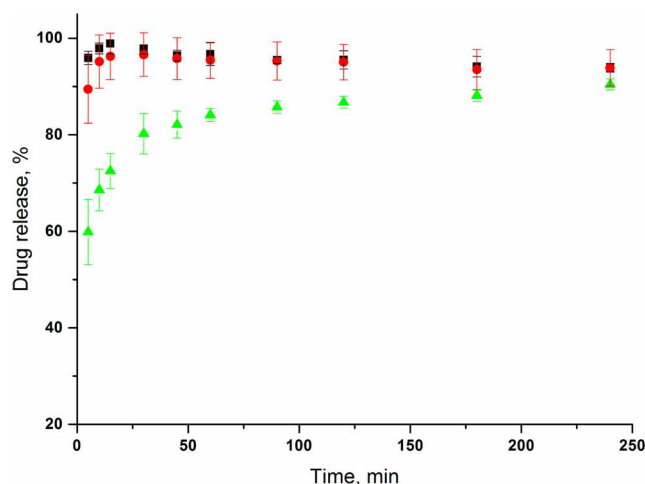


Figure 10. Drug release profile of as received ibuprofen (black squares, ■), physical mixture of ibuprofen and hydroxyapatite (red circle, ●), and hydrogen-bonded ibuprofen-hydroxyapatite complex (ibuprofen/HA) (green triangle, ▲). Slower release rate for the ibuprofen/HA complex can be clearly noted, whereas raw ibuprofen and a physical mixture of ibuprofen and HA present similar dissolution rates.

Fick's second law of diffusion.²⁴ In our case, however, we did not produce tablets, and therefore ibuprofen that formed a thin layer on the surface of the HA powder is readily released mostly from the surface rather than the bulk, thus suggesting that the profile observed in Figure 10 is not fully diffusion-controlled.

We relate this slower, and desirable, drug release to the adsorption of the API, compared to the biphasic physical mixture where the two components are not bonded to each other, thus proving that the intramolecular bonding effect between the API and a carrier is an important factor when designing materials with controlled drug release properties. The majority of the studies on combining ceramics and anti-inflammatories concentrate their attention on prolonged drug release, whereas for the treatment of arthritic patients, a "burst" drug release may be required at a point of need, followed by a prolonged drug release afterward.⁵³ Our study suggests that when ibuprofen and HA form a hydrogen-bonded complex, it may be more difficult to obtain an immediate release due to an API-carrier interaction, in turn impeding design of materials with dual properties when using the method of dissolving and recrystallizing drug in the presence of a ceramic carrier.

4. CONCLUSIONS

In this study, we elucidated the mechanism of the ibuprofen adsorption onto the surface of nanohydroxyapatite and its effects on the drug dissolution rate, explaining earlier findings on the shift of the FTIR signal of the carbonyl group of the API in the presence of ceramics. Herein, using an array of characterization tools, we demonstrated that, when synthesizing an ibuprofen/ceramic complex, hydrogen bonding occurs between the carbonyl group of the API and a Ca center of hydroxyapatite (HA). The process of surface attachment follows the steps: (i) ibuprofen dimer partial dissolution in a solvent, (ii) formation of a monomer/solvent complex from a dimer, and (iii) subsequent preferential attachment of the ibuprofen monomer to the hydroxyapatite. The latter is represented by a hydrogen bond between the hydroxyl group of ibuprofen and one of the hydroxyl groups of the HA, along with an interaction between the carbonyl group of ibuprofen

and a Ca center of HA. The formation of this complex occurs by means of first-order kinetics.

Furthermore, we have also demonstrated the influence of such noncovalent bonding on the release/dissolution rate of the drug. Through investigation of the behavior of the intramolecularly bonded ibuprofen–HA system under physiological conditions (phosphate buffer) and comparing it with the biphasic mixture of the two components, we have shown that the initial API release rate from the complex is influenced by the hydrogen-bonding-induced attachment of the ibuprofen to the surface of nanohydroxyapatite. On a wider perspective, we believe the results of this work will help to understand the effect of hydrogen bonding on the attachment of the APIs to the surface of the drug carrier and its contribution to the dissolution profile of the system.

■ ASSOCIATED CONTENT

Supporting Information

The Supporting Information is available free of charge on the ACS Publications website at DOI: 10.1021/acs.langmuir.6b04510.

ATR-FTIR spectra, SEM micrographs, molecular structures by DFT, ¹H-NMR spectra. Details of kinetics studies and equilibrium constant determination, adsorption complexes energies. Figures S1 to S19, and Table S1 (PDF)

■ AUTHOR INFORMATION

Corresponding Author

*Tel.: +44 (0) 1274 233900. E-mail: a.paradkar1@bradford.ac.uk.

ORCID

Michael F. A. Hippler: 0000-0002-3956-3922

Anant Paradkar: 0000-0003-1704-9858

Author Contributions

The manuscript was written through contributions of all authors. All authors have given approval to the final version of the manuscript.

Notes

The authors declare no competing financial interest.

■ ACKNOWLEDGMENTS

The authors would like to acknowledge funding support from EPSRC (Nos. EP/L027011/1, EP/K029592/1). This research was performed in part at the MIDAS Facility, at the University of Sheffield, which was established with support from the Department of Energy and Climate Change.

■ REFERENCES

- Vallet-Regi, M.; Gonzalez-Calbet, J. Calcium phosphates as substitution of bone tissues. *Prog. Solid State Chem.* **2004**, *32*, 1–31.
- Ogilvie, A.; Frank, R. M.; Benqué, E. P.; Gineste, M.; Heughebaert, M.; Hemmerle, J. The biocompatibility of hydroxyapatite implanted in the human periodontium. *J. Periodontol. Res.* **1987**, *22*, 270–283.
- Ryabenkova, Y.; Pinnock, A.; Quadros, P. A.; Goodchild, R. L.; Möbus, G.; Crawford, A.; Hatton, P. V.; Miller, C. A. The relationship between particle morphology and rheological properties in injectable nano-hydroxyapatite bone graft substitutes. *Mater. Sci. Eng., C* **2017**, *75*, 1083–1090.
- Hruschka, V.; Tangl, S.; Ryabenkova, Y.; Heimel, P.; Barnewitz, D.; Möbus, G.; Keibl, C.; Ferguson, J.; Quadros, P.; Miller, C.;

Goodchild, R.; Austin, W.; Redl, H.; Nau, T. Comparison of nanoparticulate hydroxyapatite pastes of different particle content and size in a novel scapula defect model. *Sci. Rep.* **2017**, *7*, 43425.

(5) Wu, G. J.; Zhou, L. Z.; Wang, K. W.; Chen, F.; Sun, Y.; Duan, Y. R.; Zhu, Y. J.; Gu, H. C. Hydroxylapatite nanorods: An efficient and promising carrier for gene transfection. *J. Colloid Interface Sci.* **2010**, *345*, 427–432.

(6) Ma, M. Y.; Zhu, Y. J.; Li, L.; Cao, S. W. Nanostructured porous hollow ellipsoidal capsules of hydroxyapatite and calcium silicate: preparation and application in drug delivery. *J. Mater. Chem.* **2008**, *18*, 2722–2727.

(7) Long, T.; Guo, Y.-P.; Liu, Y.-Z.; Zhu, Z.-A. Hierarchically nanostructured mesoporous carbonated hydroxyapatite microspheres for drug delivery systems with high drug-loading capacity. *RSC Adv.* **2013**, *3*, 24169–24176.

(8) Ueno, Y.; Futagawa, H.; Takagi, Y.; Ueno, A.; Mizushima, Y. Drug-incorporating calcium carbonate nanoparticles for a new delivery system. *J. Controlled Release* **2005**, *103*, 93–98.

(9) Wang, C.; He, C.; Tong, Z.; Liu, X.; Ren, B.; Zeng, F. Combination of adsorption by porous CaCO₃ microparticles and encapsulation by polyelectrolyte multilayer films for sustained drug delivery. *Int. J. Pharm.* **2006**, *308*, 160–167.

(10) Zhou, J.; Horev, B.; Hwang, G.; Klein, M. I.; Koo, H.; Benoit, D. S. W. Characterization and optimization of pH-responsive polymer nanoparticles for drug delivery to oral biofilms. *J. Mater. Chem. B* **2016**, *4*, 3075–3085.

(11) Ashley, G. W.; Henise, J.; Reid, R.; Santi, D. V. Hydrogel drug delivery system with predictable and tunable drug release and degradation rates. *Proc. Natl. Acad. Sci. U. S. A.* **2013**, *110*, 2318–2323.

(12) Pham, H. H.; Luo, P.; Génin, F.; Dash, A. K. Synthesis and characterization of hydroxyapatite-ciprofloxacin delivery systems by precipitation and spray drying technique. *AAPS PharmSciTech* **2002**, *3*, 1–9.

(13) Joosten, U.; Joist, A.; Gosheger, G.; Liljenqvist, U.; Brandt, B.; von Eiff, C. Effectiveness of hydroxyapatite-vancomycin bone cement in the treatment of Staphylococcus aureus induced chronic osteomyelitis. *Biomaterials* **2005**, *26*, 5251–5258.

(14) Jafari, S.; Maleki-Dizaji, N.; Barar, J.; Barzegar-Jalali, M.; Rameshrad, M.; Adibkia, K. Physicochemical characterization and in vivo evaluation of triamcinolone acetonide-loaded hydroxyapatite nanocomposites for treatment of rheumatoid arthritis. *Colloids Surf., B* **2016**, *140*, 223–232.

(15) Felson, D. T.; Lawrence, R. C.; Dieppe, P. A.; Hirsch, R.; Helmick, C. G.; Jordan, J. M.; et al. Osteoarthritis: New Insights. Part 1: The Disease and Its Risk Factors. *Ann. Intern. Med.* **2000**, *133*, 635–646.

(16) Garcia Araujo, C.; Fernandez Gonzalez, J.; Tonino, A. Rheumatoid arthritis and hydroxyapatite-coated hip prostheses. *J. Arthroplasty* **1998**, *13*, 660–667.

(17) Boureau, F.; Schneid, H.; Zeghari, N.; Wall, R.; Bourgeois, P. The IPSO study: ibuprofen, paracetamol study in osteoarthritis. A randomised comparative clinical study comparing the efficacy and safety of ibuprofen and paracetamol analgesic treatment of osteoarthritis of the knee or hip. *Ann. Rheum. Dis.* **2004**, *63*, 1028–1034.

(18) Lerdkanchanaporn, S.; Dollimore, D. A thermal analysis study of ascorbic acid and its pharmaceutical formulations. *J. Therm. Anal. Calorim.* **1997**, *49*, 879–886.

(19) Smeyers, Y. G.; Cuéllare-Rodríguez, S.; Galvez-Ruano, E.; Arias-Pérez, M. S. Conformational analysis of some α -phenylpropionic acids with anti-inflammatory activity. *J. Pharm. Sci.* **1985**, *74*, 47–49.

(20) Kierys, A.; Grochowicz, M.; Kosik, P. Fabrication of porous hollow γ -Al₂O₃ nanofibers by facile electrospinning and its application for water remediation. *Microporous Mesoporous Mater.* **2015**, *217*, 133–140.

(21) Qi, C.; Zhu, Y.-J.; Lu, B.-Q.; Zhao, X.-Y.; Zhao, J.; Chen, F. Hydroxyapatite nanosheet-assembled porous hollow microspheres: DNA-templated hydrothermal synthesis, drug delivery and protein adsorption. *J. Mater. Chem.* **2012**, *22*, 22642–22650.

(22) Melville, A. J.; Rodríguez-Lorenzo, L. M.; Forsythe, J. S. Effects of calcination temperature on the drug delivery behaviour of Ibuprofen from hydroxyapatite powders. *J. Mater. Sci.: Mater. Med.* **2008**, *19*, 1187–1195.

(23) Sambudi, N. S.; Chob, S.; Cho, K. Porous hollow hydroxyapatite microspheres synthesized by spray pyrolysis using a microalga template: Preparation, drug delivery, and bioactivity. *RSC Adv.* **2016**, *6*, 43041–43048.

(24) Öner, M.; Yetiz, E.; Ay, E.; Uysal, U. Ibuprofen release from porous hydroxyapatite tablets. *Ceram. Int.* **2011**, *37*, 2117–2125.

(25) Kumar, R.; Prakash, K. H.; Cheang, P.; Khor, K. A. Temperature driven morphological changes of chemically precipitated hydroxyapatite nanoparticles. *Langmuir* **2004**, *20*, 5196–5200.

(26) Cullity, B. D.; Stock, S. R. In *Elements of X-Ray Diffraction*, 3rd Edition; Prentice-Hall: Upper Saddle River, NJ, 2001; p 236.

(27) Mohr, C.; Spencer, C. L.; Hippler, M. Inexpensive Raman spectrometer for undergraduate and graduate experiments and research. *J. Chem. Educ.* **2010**, *87*, 326–330.

(28) www.webbook.nist.gov; accessed March 23, 2016.

(29) Frisch, M. J.; Trucks, G. W.; Schlegel, H. B.; Scuseria, G. E.; Robb, M. A.; Cheeseman, J. R.; Scalmani, G.; Barone, V.; Mennucci, B.; Petersson, G. A.; Nakatsuji, H.; Caricato, M.; Li, X.; Hratchian, H. P.; Izmaylov, A. F.; Bloino, J.; Zheng, G.; Sonnenberg, J. L.; Hada, M.; Ehara, M.; Toyota, K.; Fukuda, R.; Hasegawa, J.; Ishida, M.; Nakajima, T.; Honda, Y.; Kitao, O.; Nakai, H.; Vreven, T.; Montgomery, J. A., Jr.; Peralta, J. E.; Ogliaro, F.; Bearpark, M. J.; Heyd, J.; Brothers, E. N.; Kudin, K. N.; Staroverov, V. N.; Kobayashi, R.; Normand, J.; Raghavachari, K.; Rendell, A. P.; Burant, J. C.; Iyengar, S. S.; Tomasi, J.; Cossi, M.; Rega, N.; Millam, N. J.; Klene, M.; Knox, J. E.; Cross, J. B.; Bakken, V.; Adamo, C.; Jaramillo, J.; Gomperts, R.; Stratmann, R. E.; Yazyev, O.; Austin, A. J.; Cammi, R.; Pomelli, C.; Ochterski, J. W.; Martin, R. L.; Morokuma, K.; Zakrzewski, V. G.; Voth, G. A.; Salvador, P.; Dannenberg, J. J.; Dapprich, S.; Daniels, A. D.; Farkas, O.; Foresman, J. B.; Ortiz, J. V.; Cioslowski, J.; Fox, D. J. *Gaussian 09, Revision D.01*; Gaussian, Inc.: Wallingford, CT, 2009.

(30) Stephens, P.; Devlin, F.; Chabalowski, C.; Frisch, M. J. Ab Initio calculation of vibrational absorption and circular dichroism spectra using density functional force fields. *J. Phys. Chem.* **1994**, *98*, 11623–11627.

(31) Narbutt, J.; Oziminski, W. P. Selectivity of bis-triazinyl bipyridine ligands for americium(III) in Am/Eu separation by solvent extraction. Part 1. Quantum mechanical study on the structures of BTBP complexes and on the energy of the separation. *Dalton Trans.* **2012**, *41*, 14416–14424.

(32) Ahrens, T.; Ahrens, M.; Braun, T.; Braun, B.; Herrmann, R. Synthesis of a rhodium(I) germyl complex: A useful tool for C–H and C–F bond activation reactions. *Dalton Trans.* **2016**, *45*, 4716–4728.

(33) Andersson, M. P.; Uvdal, P. New scale factors for harmonic vibrational frequencies using the B3LYP density functional method with the triple- ζ basis set 6-311+G(d,p). *J. Phys. Chem. A* **2005**, *109*, 2937–2941.

(34) Liao, C.-J.; Lin, F.-H.; Chen, K.-S.; Sun, J.-S. Thermal decomposition and reconstitution of hydroxyapatite in air atmosphere. *Biomaterials* **1999**, *20*, 1807–1813.

(35) Gulley-Stahl, H.; Hogan, P. A.; Schmidt, W. L.; Wall, S. J.; Buhrlage, A.; Bullen, H. A. Surface complexation of catechol to metal oxides: An ATR-FTIR, adsorption, and dissolution Study. *Environ. Sci. Technol.* **2010**, *44*, 4116–4121.

(36) Jabbari, E.; Wisniewski, N.; Peppas, N. A. Evidence of mucoadhesion by chain interpenetration at a poly(acrylic acid)/mucin interface using ATR-FTIR spectroscopy. *J. Controlled Release* **1993**, *26*, 99–108.

(37) Huang, L. Y.; Xu, K. W.; Lu, J. Bone healing in porous implants. An experiment in sheep. *J. Mater. Sci.: Mater. Med.* **2000**, *11*, 667–673.

(38) Lim, G. K.; Wang, J.; Ng, S. C.; Gan, L. M. Nanosized hydroxyapatite powders from microemulsions and emulsions stabilized by a biodegradable surfactant. *J. Mater. Chem.* **1999**, *9*, 1635–1639.

(39) Gibson, I. R.; Rehman, I.; Best, S. M.; Bonfield, W. Characterization of the transformation from calcium-deficient apatite

to beta-tricalcium phosphate. *J. Mater. Sci.: Mater. Med.* **2000**, *11*, 799–804.

(40) Viswanath, B.; Ravishankar, N. Controlled synthesis of plate-shaped hydroxyapatite and implications for the morphology of the apatite phase in bone. *Biomaterials* **2008**, *29*, 4855–4863.

(41) Gibson, I. R.; Bonfield, W. Novel synthesis and characterization of an AB-type carbonate-substituted hydroxyapatite. *J. Biomed. Mater. Res.* **2002**, *59*, 697–708.

(42) Ibrahim, D. M.; Mostafa, A. A.; Korowash, S. I. Chemical characterization of some substituted hydroxyapatites. *Chem. Cent. J.* **2011**, *5*, 74.

(43) Chevalier, E.; Viana, M.; Cazalbou, S.; Makein, L.; Dubois, J.; Chulia, D. Ibuprofen-loaded calcium phosphate granules: Combination of innovative characterization methods to relate mechanical strength to drug location. *Acta Biomater.* **2010**, *6*, 266–274.

(44) Talmon, Y. Electron Beam Radiation Damage to Organic and Biological Cryospecimens. In *Cryotechniques in Biological Electron Microscopy*; Steinbrecht, R. A., Zierold, K., Eds.; Springer-Verlag: Berlin, Heidelberg, 1987; pp 64–84.

(45) Rangavittal, N.; Landa-Cánovas, A. R.; González-Calbet, J. M.; Vallet-Regí, M. Structural study and stability of hydroxyapatite and β -tricalcium phosphate: Two important bioceramics. *J. Biomed. Mater. Res.* **2000**, *51*, 660–668.

(46) Vueba, M. L.; Pina, M. E.; Batista de Carvalho, L. A. Conformational stability of ibuprofen: Assessed by DFT calculations and optical vibrational spectroscopy. *J. Pharm. Sci.* **2008**, *97*, 845–859.

(47) Williamson, M. P. Using chemical shift perturbation to characterise ligand binding. *Prog. Nucl. Magn. Reson. Spectrosc.* **2013**, *73*, 1–16.

(48) Levitt, M.; Perutz, M. F. Aromatic rings act as hydrogen bond acceptors. *J. Mol. Biol.* **1988**, *201*, 751–754.

(49) Penel, G.; Leroy, G.; Rey, C.; Sombret, B.; Huvenne, J. P.; Bres, E. Infrared and Raman microspectroscopy study of fluor-fluor-hydroxy- and hydroxyl-apatite powder. *J. Mater. Sci.: Mater. Med.* **1997**, *8*, 271–276.

(50) Zhan, C.-H.; Jiang, M.-X.; Feng, Y.-L.; He, Y.-H. Syntheses, structures, network topologies and photoluminescence of four Zn(II) and Cd(II) coordination polymers based on 5-carboxyl-1-carboxymethyl-2-oxypyridinium. *Polyhedron* **2010**, *29*, 2250–2257.

(51) Aroca, R.; Jennings, C.; Loutfy, R. O.; Hor, A. M. The structure of organic thin films: Raman polarization studies. *J. Phys. Chem.* **1986**, *90*, 5255–5257.

(52) Hédoux, A.; Guinet, Y.; Derollez, P.; Dudognon, E.; Correia, N. T. Raman spectroscopy of racemic ibuprofen: Evidence of molecular disorder in phase II. *Int. J. Pharm.* **2011**, *421*, 45–52.

(53) Hite, M.; Federici, C.; Brunelle, A.; Turner, S. *Modified release ibuprofen dosage form*. U.S. Patent No. US9028869 B2, 2015.